ICARUS **130,** 165–176 (1997)
ARTICLE NO. IS975804

Constraints on Spin State and Hapke Parameters of Asteroid 4769 Castalia Using Lightcurves and a Radar-Derived Shape Model

R. Scott Hudson

School of Electrical Engineering and Computer Science, Washington State University, Pullman, Washington 99164-2752
E-mail: hudson@eecs.wsu.edu

Steven J. Ostro and Alan W. Harris

Jet Propulsion Laboratory, California Institute of Technology, Pasadena, California 91109-8099

Received October 21, 1996; revised April 18, 1997

A 167-parameter, 3-D shape model of the Earth-crossing asteroid Castalia, obtained from inversion of delay-Doppler images (Hudson and Ostro, 1994, *Science* 263, 940–943) constrained the object's pole to lie on a cone of half angle 55 ± 10° centered on the radar line of sight (right ascension 0.3 hr, declination 25.4°) at the time of observations (Aug. 22, 1989) but could not constrain the pole's azimuthal orientation or the sense of rotation. Here we fit lightcurves obtained at Table Mountain Observatory on Aug. 23–25 with lightcurves calculated from Castalia's shape and Hapke's photometric model (Hapke 1981, *J. Geophys. Res.* 86, 3039–3054; 1984, *Icarus* 59, 41–59; 1986, *Icarus* 67, 264–280). The fits strongly constrain Castalia's spin state to one of two possibilities. One has a north pole within ~13° of $\lambda = 253°$, $\beta = 56°$ and a sidereal spin period $P = 4.089 \pm 0.001$ hr. The other has a south pole within ~13° of $\lambda = 242°$, $\beta = 7°$ and a sidereal spin period $P = 4.094 \pm 0.001$ hr. The north-pole solution has global-average Hapke photometric parameters $w = 0.38 \pm 0.07$, $g = -0.11 \pm 0.09$, $\overline{\theta} = 46° \pm 10°$ while the south-pole solution has $w = 0.24 \pm 0.07$, $g = -0.30 \pm 0.09$, $\overline{\theta} = 25° \pm 10°$. Due to the large solar phase angles (60°–90°) the fits are not sensitive to the opposition surge parameters h and B_0. At a more subtle level, the least-bifurcated shape ("lower-bound model") allowed by the radar data (Hudson and Ostro, 1994, *Science* 263, 940–943) consistently gives statistically better fits than the more bifurcated possibilities. However, the differences are small enough that the possibility that they are due to unmodeled photometric effects cannot be discounted. The fits are improved by allowing the macroscopic roughness parameter $\overline{\theta}$ to be a function of surface position. Statistically, this process improves the north-pole solution more than the south-pole solution suggesting that the radar observations viewed a northern latitude, thereby indicating a resolution of the "mirror ambiguity" inherent in the single-date radar data set. © 1997 Academic Press

Key Words: asteroids; photometry; radar; surfaces.

1. INTRODUCTION

It has long been clear that the asteroid population is immense, extremely diverse, and has a range of sizes that virtually guarantees an abundance of irregular shapes and a wide range of pole directions under any conceivable evolutionary scenario. Yet these objects are tantalizingly unresolvable to ground-based optical telescopes. Not surprisingly then, the relation between lightcurves and an asteroid's shape and spin state has been a subject of interest for nearly a century. In the absence of spatially resolved observations these data are the only source of geometric leverage for such investigations, yet the fundamental limitations of lightcurves in this respect has been apparent for some time (Russell 1906). As a result, most lightcurve inversion techniques have been based on simple models such as homogeneous ellipsoids and two-dimensional averages of the shape (Magnusson *et al.* 1989).

Most of these techniques have been developed for use with mainbelt asteroid lightcurves taken near opposition, hence at small solar phase angles, in which case brightness variations can be reasonably interpreted as representing changes in projected area, as near zero solar phase shadowing is not a major concern. On the other hand, at the high solar-phase angles that are common in near-Earth asteroid observations, shadowing due to details of the shape will necessarily be a major factor in the determination of the lightcurve shape, and the interpretation of a lightcurve becomes more complicated.

The availability of spatially resolved images broadens the range of possibilities. At one extreme, an extended spacecraft rendezvous could conceivably provide such complete shape and photometric information as to render Earth-based lightcurves superfluous. For spacecraft flybys

0019-1035/97 $25.00

that provide incomplete image coverage (Thomas *et al.* 1994, 1996; Helfenstein *et al.* 1994, 1996) lightcurves can help constrain poorly imaged areas, refine spin periods (Simonelli *et al.* 1995), and confirm the accuracy of shape and photometric models (Simonelli *et al.* 1996).

A situation intermediate between spacecraft scenarios and lightcurve data sets arises when an independent observational technique, such as radar, can provide substantial, but incomplete, information about shape and spin state. In such cases synergy between these data and lightcurves has the potential to provide significant improvement in the physical characterization of the asteroid. Situations of this sort can be expected to arise with increasing frequency in the near future (Ostro 1993). In this paper we investigate the use of lightcurves in conjunction with a radar-derived shape model to characterize asteroid 4769 Castalia.

2. SHAPE MODELS

Castalia (formerly 1989 PB) was discovered 9 August 1989 by E. F. Helin at Palomar Observatory and was observed by radar for a 2.5 hr period centered on 22 August 1989 06:45:00 UTC (Ostro *et al.* 1989) when its plane-of-sky (POS) position was right ascension 0.3 hr and declination 25.4°. This observation produced 64 delay-Doppler images, each with a resolution of 300 m in range and approximately 180 m along the Doppler axis, and covered approximately 220° of rotational phase.

Hudson and Ostro (1994) inverted these data to obtain two shape models that represent lower and upper bounds on the degree of Castalia's bifurcation, and they adopted an intermediate shape as a nominal working model. Figure 1 shows silhouettes from pole-on, ''end-on,'' ''broadside,'' and of the ''contact region'' between the lobes for these ''lower-bound,'' ''nominal,'' and ''upper-bound'' models. We note that the models vary least in the north and on the side that had the best rotation phase coverage. This is clear from both the pole-on and broadside silhouettes and particularly from the changes in the ''contact region.'' Most of the variation between the models occurs in the south and on the less well-imaged side. This is not surprising given that the radar had a northern view and the phase coverage was incomplete, resulting in poorer constraints in the south and on the side with poor phase coverage.

The radar data inversion also constrained the absolute value of the asteroid-centered declination of the Earth to be 35° ± 10°, or equivalently, constrained the north or south pole to lie on a cone of half angle 55° ± 10° centered on the radar line-of-sight. As discussed below, a single-date radar set cannot constrain either the azimuthal orientation of the pole on the POS or the sense of rotation, leaving a ''mirror ambiguity'' in the shape.

The availability of lightcurves raised interesting possibilities. First, they might provide an important and independent verification of the shape model. If it proved impossible to explain the lightcurves using the radar-derived shape then that result would be suspect; if it proved possible, then would this process tend to favor either the upper or lower bounds on Castalia's bifurcation? Second, could lightcurves provide the geometric leverage needed to constrain the azimuthal orientation of the pole and the sense of rotation? Finally, could the photometric properties of Castalia's surface be accurately modeled? These are the questions we investigate in this paper. We begin with a discussion of some of the geometrical aspects of the radar and lightcurve observations.

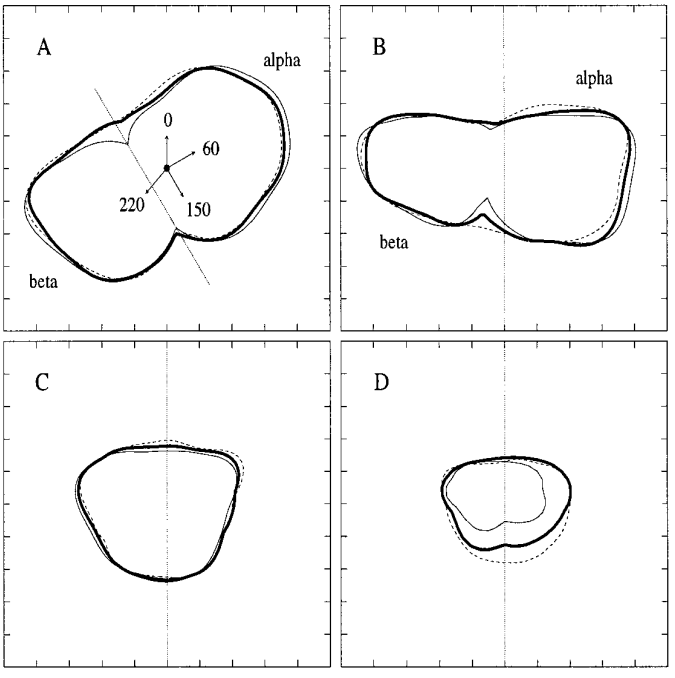

FIG. 1. Projections of Castalia models. Dashed curve, thick solid curve, and thin solid curve, correspond to, respectively, lower-bound, nominal, and upper-bound models. (A) Pole-on view. The four arrows are joined at the pole and point in the direction of rotational phases ψ shown. (B) Broadside view from $\psi = 150°$. (C) End-on view from $\psi = 60°$. (D) Cross sections along the dotted line in (A), the ''contact region.'' The tick spacing is 200 m. In Figs. B, C, and D the spin axis is indicated by a dotted line.

3. OBSERVATIONAL GEOMETRY

Consider the geometry illustrated in Fig. 2. The (x_0, y_0, z_0) system is an asteroid-centered inertial system, and we choose the z_0 direction to coincide with the line-of-sight during the radar observations. This is valid if the POS motion is negligible during this time interval, as it was for Castalia (less than 1° of motion). The (x, y, z) system is fixed on the asteroid with the pole lying along the z axis. The Euler angles ϕ, θ, ψ orient the asteroid coordinates

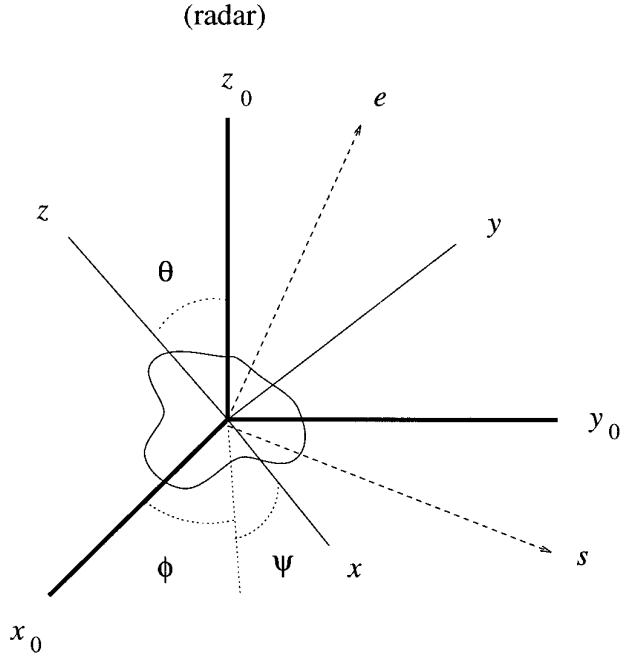

FIG. 2. Observational geometry.

with respect to the inertial system (Landau and Lifshitz 1976). The pole direction is specified by ϕ and θ; $\psi = (2\pi/P)t$ is the rotation phase with P the sidereal spin period.

The radar time delay τ of a point (x, y, z) on the asteroid with respect to the center of mass (COM) is proportional to the z_0 coordinate of the point. The Doppler frequency ν relative to the COM is proportional to the time derivative of τ provided we can neglect the orbital contribution to the apparent spin vector. This is valid if the rotational angular velocity of the asteroid is much larger than the orbital angular velocity relative to Earth. (In Castalia's case these were 2114°/day and ~10°/day, respectively.) If the surface normal at the point is $\hat{n} = (n_x, n_y, n_z)$ then the cosine of the incidence angle i, which determines the radar brightness of the point, is the projection of $\hat{n}$ along the z_0 axis. These three quantities are what determine each point's contribution to a delay-Doppler image, and they have the values

$$\tau = -\frac{2}{c}[z\cos\theta + (x\sin\psi + y\cos\psi)\sin\theta]$$

$$\nu = -\frac{2}{\lambda_r}\frac{2\pi}{P}(x\cos\psi - y\sin\psi)\sin\theta$$

$$\cos i = n_z\cos\theta + (n_x\sin\psi + n_y\cos\psi)\sin\theta$$

with c the speed of light and λ_r the radar wavelength. These equations depend on θ; in particular Doppler frequency is proportional to $\sin\theta$, so delay-Doppler images are sensitive to this component of the pole's direction. (For Castalia $|\theta| = 55° \pm 10°$.) However, there is no dependence on ϕ, so a single-date radar data set cannot constrain the azimuthal component of an asteroid's pole. Another way of saying this is that changing ϕ is equivalent to rotating the radar about the line of sight, but the radar system has circular symmetry about this line so the delay-Doppler image will not change.

Now, suppose we mirror image the model through the y–z plane, i.e., $(x, y, z) \mapsto (-x, y, z)$ and $(n_x, n_y, n_z) \mapsto (-n_x, n_y, n_z)$, and we reverse the sense of rotation $P \mapsto -P$ (hence $\psi \mapsto -\psi$). The values of τ, ν, and $\cos i$ are unchanged, so the same delay-Doppler image will be obtained as before. Therefore a single-date radar data set will always permit a two-fold "mirror ambiguity" in the shape corresponding to an unknown sense of rotation. We will refer to the shape corresponding to $P > 0$, hence with the z axis being the north pole, as the northern version, and that corresponding to $P < 0$, in which case the z axis becomes the south pole, as the southern version. Hudson and Ostro (1994) noted this ambiguity and presented northern versions of the shapes.

If a nonzero-phase lightcurve is obtained at the same time as the radar observation then the symmetry about the z_0 axis will be broken and the lightcurves might be sensitive to ϕ. In Fig. 2 let $\hat{s}$ be the direction of the Sun and choose the (arbitrary) orientation of the x_0 and y_0 axes so that $\hat{s}$ lies in the y_0, z_0 plane. An examination of the equations of transformation between asteroid and inertial coordinates shows that letting $(x, y, z) \mapsto (-x, y, z)$, $\psi \mapsto -\psi$, and $\phi \mapsto -\phi$ results in $(x_0, y_0, z_0) \mapsto (-x_0, y_0, z_0)$. Therefore, the projections of any position vector or surface normal along the directions of the Earth and of the Sun (which are insensitive to the sign of the x_0 component) as functions of time are unchanged, and the delay-Doppler images and the lightcurve will be unchanged. It follows that the mirror ambiguity cannot be resolved with a combination of radar and lightcurve data on a single date, and there will be a corresponding two-fold ambiguity in ϕ. These same considerations apply if $\hat{s}$ denotes the direction of the radar on a different date for which delay-Doppler images are obtained, so we can also state that the mirror ambiguity cannot be resolved from two dates of radar observations. (Note that by "the lightcurve will be unchanged" we are referring to the shape of the lightcurve and not the subtle temporal effects that form the basis of the Epoch Method (Magnusson *et al.* 1989).

In order to have a possibility of resolving the mirror ambiguity we need observations which include a third direction. For example, suppose that the z_0 axis is the direction of the radar on the date of a delay-Doppler observation, and $\hat{s}$ and $\hat{e}$ are the directions of the Sun and Earth during a lightcurve observation on another date. If $\hat{e}$ is not

coplanar with $\hat{s}$ and $\hat{z}_0$, i.e., if it has an x_0 component, then the mirror imaging operation will, in principle, change the lightcurve viewed along the $\hat{e}$ direction and it might be possible to resolve the mirror ambiguity. The same situation holds for three radar observations.

If the asteroid's orbital inclination were 0°, then the Earth and Sun would always lie in a common plane when viewed from the asteroid and this type of geometric leverage would never arise. Significant leverage requires the geometric diversity resulting from a nonzero inclination coupled with one or more close Earth approaches. For this reason this technique is likely to be of limited use for mainbelt objects.

4. MODEL FITS

Castalia was observed at Table Mountain Observatory (TMO) on three nights, August 23, 24, and 25, 1989. The observers at the telescope were James Young and Bonnie Wallace. The observations were made with a single channel photoelectric photometer on the 0.6-m TMO telescope. Details of the observing system and data reduction are given by Harris and Young (1983) and Harris and Lupishko (1989). Observations were reduced to V band magnitudes of the Johnson and Morgan system, with further reduction to 1 AU Earth and Sun distances. Small corrections were made to correct all magnitudes to the standard phase angles at the mid-time of each lightcurve, as listed in Table I. Observation times were light-time corrected, so that the times refer to time on the asteroid. A data file containing individual times and magnitude measurements is available from A. Harris or may be obtained from the *Asteroid Photometric Catalog* (Lagerkvist *et al.* 1987 and subsequent updates).

The angular positions in ecliptic coordinates of the Sun and Earth as viewed from Castalia are shown in Fig. 3. The large solar phase angles imply that the lightcurves will provide firm constraints on the azimuthal angle ϕ in Fig. 2. However, the four Earth positions are essentially coplanar, so the only geometric leverage for resolving the mirror ambiguity is the ~20° separation of the solar positions from this plane. This separation is fairly modest implying that this leverage will not be very strong.

From Castalia and solar ephemerides we knew the Sun–Earth–Castalia geometry at all times of interest. For an assumed pole direction we could solve for the Castalia-centered declination and right ascension of the Earth and

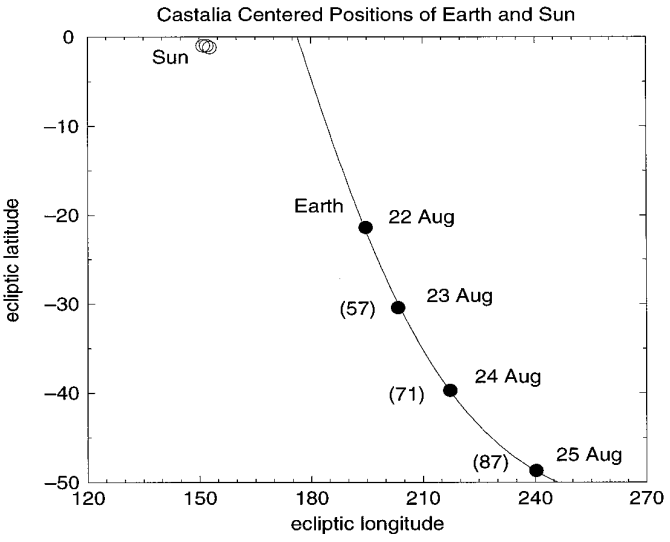

FIG. 3. Sun–Castalia–Earth geometry. Aug. 22 position of Earth corresponds to radar observations and z_0 axis of Fig. 2. Curve shows best-fit plane for Earth positions. Numbers in parentheses are solar phase angles.

the Sun and thereby the illumination and observation orientations. Then, for a given shape model, tracing rays from the Sun to the asteroid to the Earth allowed us to map out the visible, illuminated portion of the surface and calculate the incidence, emergence and phase angles i, e, and α as a function of surface position. Applying the Hapke photometric function $r(i, e, \alpha)$ (Hapke 1981, 1984, 1986) then produced spatially resolved POS images, and disc integrations provided absolute lightcurve magnitude as a function of time.

We considered six candidate models: lower-bound, nominal, and upper-bound models each in northern and southern versions. Each of the six models was constructed as a collection of 796 roughly equal-area surface facets. POS images were rendered at a resolution of 20 × 20 m for most of the fits and then at 10 × 10 m for final refinements. Separate raytracings were done for each of the 226 lightcurve data points.

With 226 data points and only a few free parameters, the distribution of χ^2 will be nearly Gaussian with mean $\mu \sim 220$ and standard deviation $\sigma \sim \sqrt{440}$. The ratio $\sigma/\mu \sim 10\%$, so a fractional change in χ^2 of this amount is beginning to become "statistically significant." We use this fact in our inferences below.

4.1. Grid Search

Our first series of calculations was a grid search over the region of possible pole directions for each of the six candidate models. We fixed the aspect angle corresponding to the time of radar observations at its radar-constrained value of 55° and then allowed the azimuthal angle ϕ of

TABLE I
Geometry of Castalia Lightcurve Observations

Date (UT)	R.A.	Dec.	Long.	Lat.	r	Δ	α	$V(\alpha)$
89/8/23.3	$0^h35.3^m$	36°51′	355.7°	17.2°	1.0278	0.0318	57.64°	19.631 ± 0.004
89/8/24.3	$1^h07.7^m$	51°34′	0.5°	24.2°	1.0195	0.0281	71.54°	20.099 ± 0.004
89/8/25.4	$2^h43.3^m$	68°51′	6.8°	33.7°	1.0102	0.0270	90.26°	20.847 ± 0.008

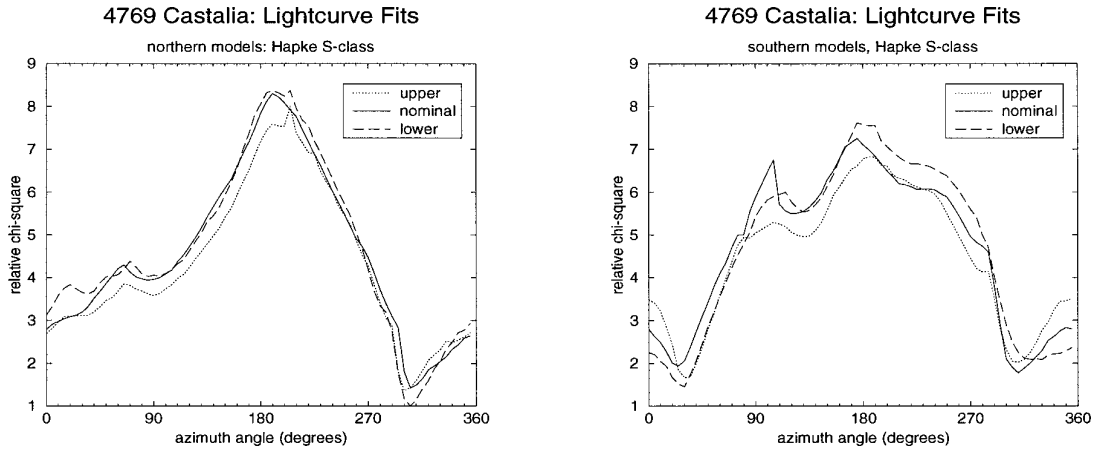

FIG. 4. Fit error vs azimuth angle of pole for six candidate models. A homogeneous Hapke photometric function with nominal S-class parameters was used. The value of χ^2 was normalized to its minimum value over all the fits.

the pole to vary in 5° steps around the cone of possible pole directions. The orientation of the asteroid about its spin axis at the (arbitrary) initial time was a free parameter. Two initial values of this parameter, differing by 180°, were used to avoid problems with local minima. Each model was given a homogeneous Hapke photometric function with nominal S-class parameters, i.e., $w = 0.23$, $h = 0.02$, $B_0 = 1.32$, $g = -0.35$, $\overline{\theta} = 20°$ (Helfenstein *et al.* 1994). The resulting χ^2 errors are shown in Fig. 4. The best fit was provided by the northern lower-bound model. Given that a fractional variation of 0.1 in χ^2 is significant, it is clear from the distinct minima in these plots that even a few days of lightcurve observations can provide the geometric leverage needed to constrain the azimuthal pole orientation left unconstrained by the radar observations.

These minima provided us with initial conditions from which to execute more refined fits. The northern model curves display single minima while there are double minima for the southern models. In the calculations described below we investigated both sets of candidate initial conditions for the southern models. The northern models also provide better fits for nominal S-class parameters. It is also clear from these plots that while the lightcurve fits are quite sensitive to the pole direction, they are much less sensitive to details of the asteroid's shape.

4.2. Homogeneous Models

The next step was to repeat the fits for the six best-fit, S-class models while floating the parameters of the spin states and homogeneous photometric functions. Given the large phase angles (between about 60° and 90°) it is not surprising that the lightcurve fits showed no significant sensitivity to the lightcurve opposition parameters h and B_0. We therefore fixed $B_0 = 0$ in all the fits (h then ceases to affect the photometric function), i.e., we ignored opposition effects. This leaves just the three photometric parameters w, g, and $\overline{\theta}$. Figure 5 shows the resulting six best fits. Table II gives the corresponding values of spin state, photometric parameters, and χ^2 with uncertainties estimated from the dispersion of values. The χ^2 values are normalized to the best fit which had an rms error of 0.1 mag. At a statistically significant level, these fits favor the lower-bound models but do not clearly distinguish between the northern and southern versions.

We adopt the lower-bound model parameters as two candidate solutions for the spin state and global-average photometric function. Although the two models give similar values for χ^2, the northern model interprets the surface as being relatively brighter and rougher while the southern model interprets the surface as relatively darker and smoother. The Hapke parameters of the southern model are quite similar to Dactyl's ($w = 0.211$, $g = -0.33$, $\overline{\theta} = 23°$) (Helfenstein *et al.* 1996). Those of the northern model are somewhat similar to Gaspra's ($w = 0.36$, $g = -0.18$, $\overline{\theta} = 29°$) (Helfenstein *et al.* 1994), the main difference being the very large value of $\overline{\theta}$. Therefore, one can imagine that Castalia's surface may be very similar to Dactyl's or that it might be similar to Gaspra's at the microscopic level but much rougher at the macroscopic level.

Although the northern and southern lower-bound models give almost equally good values of χ^2, Fig. 5 shows that the modeled lightcurves themselves are distinctly different. The southern model displays large deviations at the first two extrema of the Aug. 24 data while the residuals of the northern model are more evenly spread throughout the data. These differences imply that the two models are not redundant and a more detailed photometric model might be able to choose between them. Therefore, in the next section we investigate the possibility of inhomogeneous surface properties.

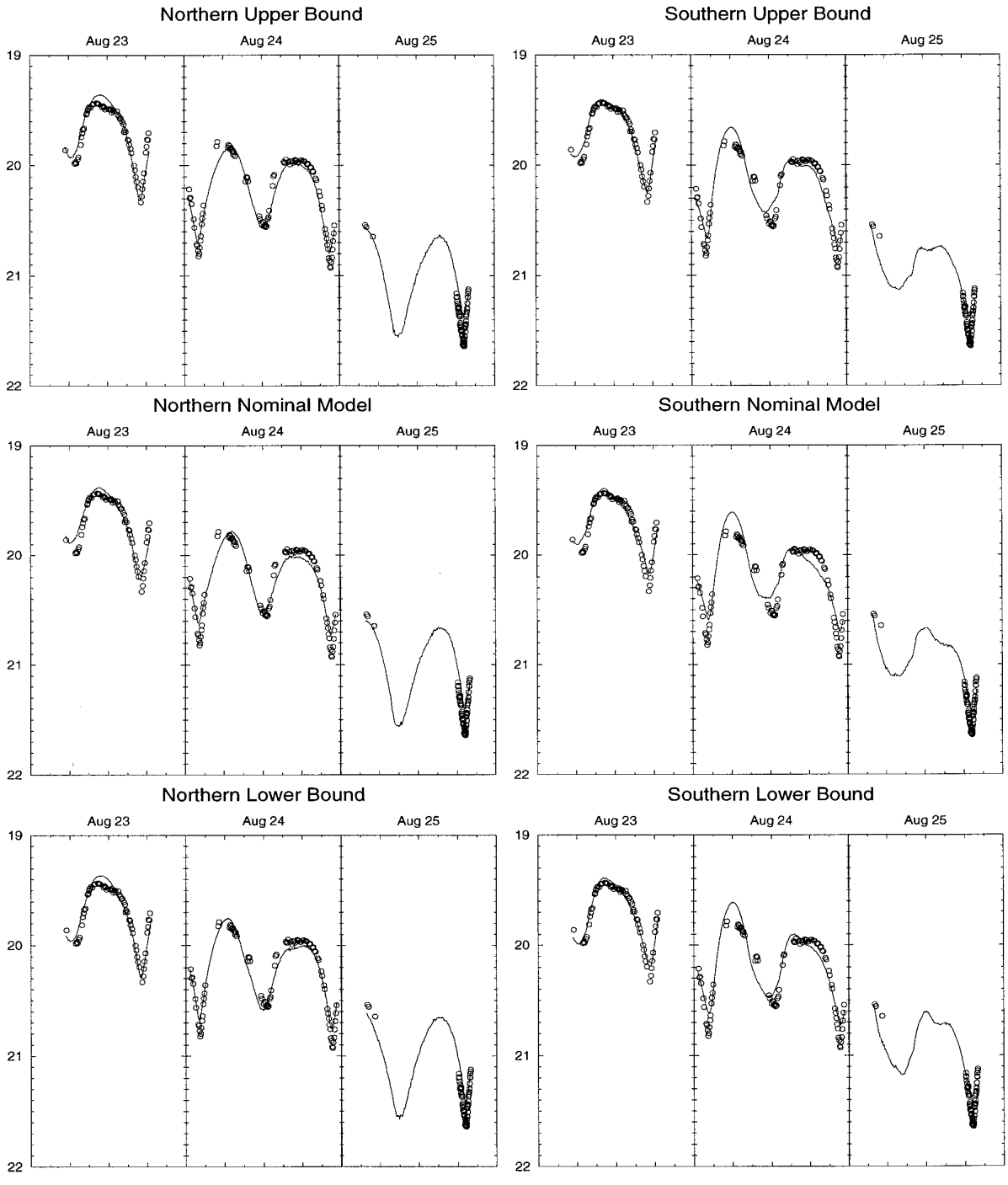

FIG. 5. Best fits, with respect to spin state and photometric parameters, for uniform Hapke photometric function. Absolute magnitude is plotted vs time with 0.2 days shown on each date. Circles are observed data; curves are fits.

4.3. Inhomogeneous Models

Galileo imaging results for Gaspra (Belton *et al.* 1992, Helfenstein *et al.* 1994) showed variations in photometric properties across its surface. Simonelli *et al.* (1995) found evidence in discrepancies between modeled and observed Gaspra lightcurves for possible surface variations in macroscopic roughness but not for albedo variations. For a kilometer-sized object like Castalia one could argue that a homogeneous distribution of particle properties is plausi-

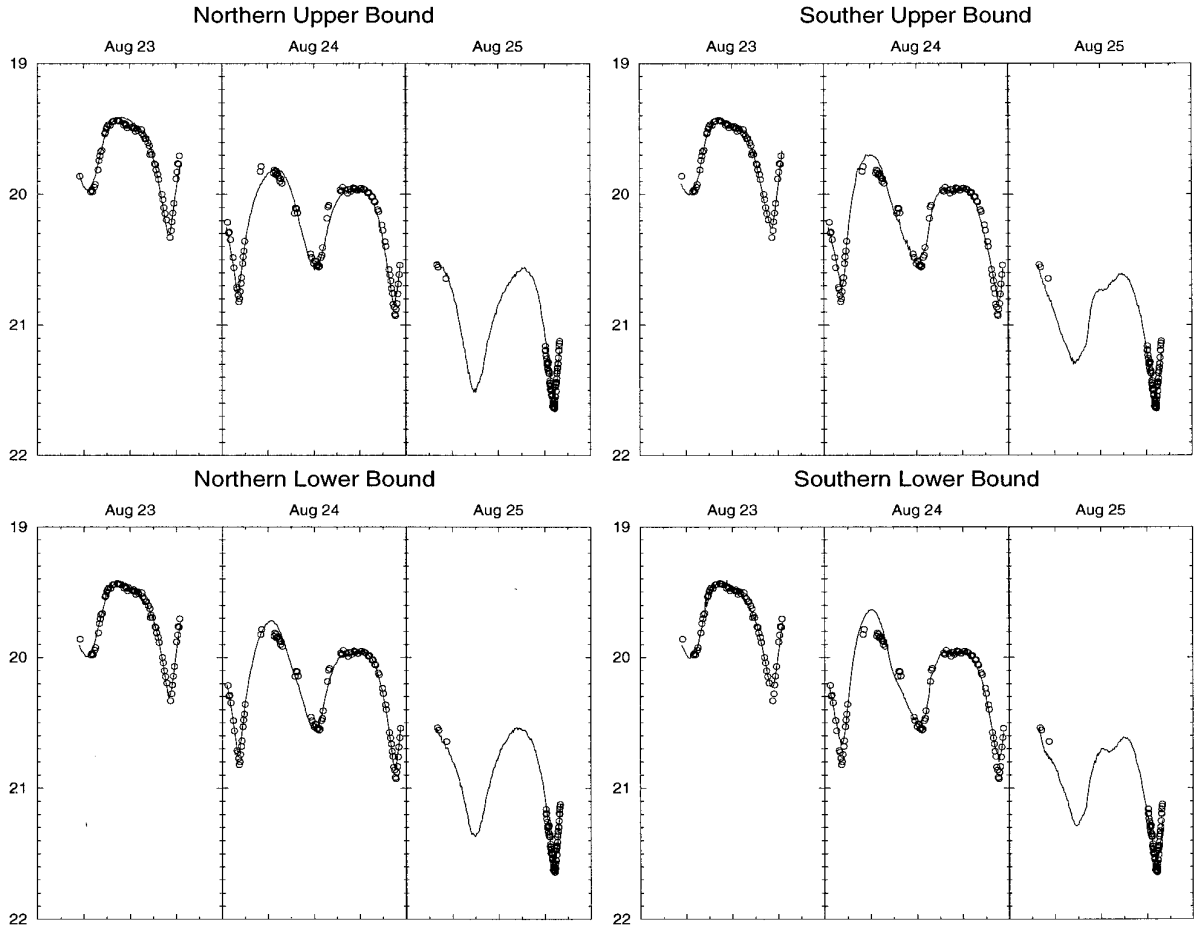

FIG. 6. Best fits with inhomogeneous Hapke photometric function.

ble. In other words, a photometric model in which the single-scattering particle parameters w and g are homogeneous seems reasonable. However, it seems difficult to make a plausible argument that the macroscopic roughness $\overline{\theta}$ would necessarily be homogeneous. Therefore, we investigated inhomogeneous photometric functions in which w and g were global but $\overline{\theta}$ was allowed to vary for each of the 796 surface facets. We considered both the lower- and upper-bound models to test if the fits would still be sensitive to differences in shape given the large number of degrees of freedom afforded by the inhomogeneous photometric functions.

A penalty function that tended to minimize the fractional standard deviation of $\overline{\theta}$ allowed this distribution to be forced as close to uniform as desired. Various weightings

TABLE II
Spin-State and Photometric Parameters for Best-Fit Homogeneous Models

Pole	Model	$\lambda°$	$\beta°$	P (hr)	w	g	$\bar{\theta}°$	χ^2
north	upper	250	-43	4.087659	0.317	-0.200	36	1.32
north	nominal	252	-45	4.088560	0.310	-0.200	35	1.29
north	lower	253	-56	4.089125	0.384	-0.112	46	1.00
south	upper	243	2	4.094799	0.271	-0.267	32	1.18
south	nominal	243	7	4.090974	0.244	-0.302	25	1.76
south	lower	242	7	4.094117	0.239	-0.299	25	1.06
	(uncertainty)	±13		±0.001	±0.07	±0.09	±10	

TABLE III
Spin-State and Photometric Parameters for Best-Fit Inhomogeneous Models

Pole	Model	$\lambda°$	$\beta°$	P hr	w	g	$\bar{\theta}°$	χ^2
north	upper	251	-43	4.087655	0.303	-0.240	38 ± 13	1.53
north	lower	253	-56	4.087640	0.377	-0.081	46 ± 14	1.00
south	upper	243	2	4.094134	0.275	-0.246	35 ± 11	1.63
south	lower	242	7	4.095267	0.274	-0.243	34 ± 10	1.74

FIG. 7. Surface distribution of $\bar{\theta}$. Top row, northern model; bottom row, mirror image of southern model. Rotation phase increases by 90° from column to column.

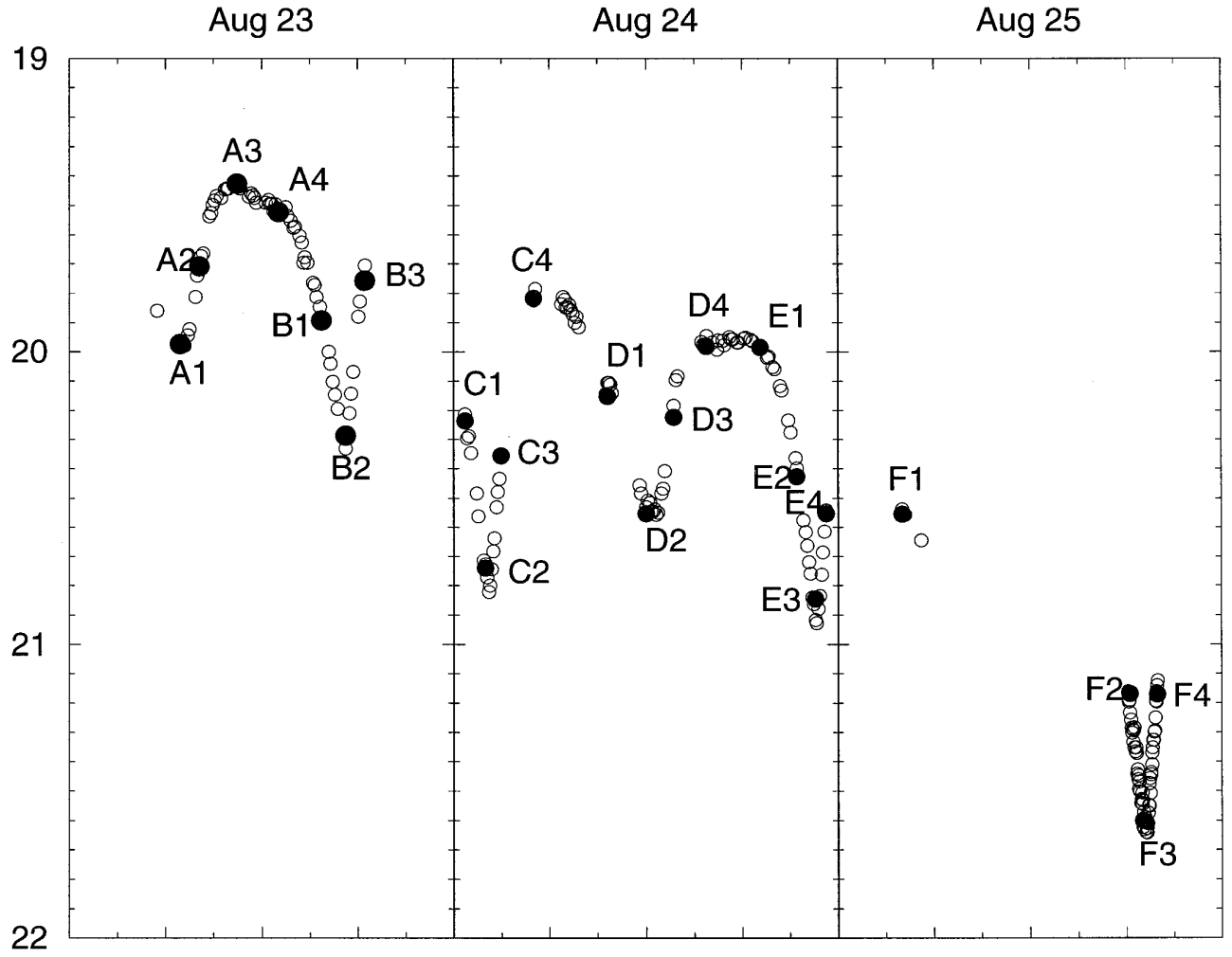

FIG. 8. Observed data (open circles) and selected fit data (filled circles) for inhomogeneous northern lower-bound model. Labels denote rows (letters) and columns (numbers) of Fig. 9.

of this penalty were tried and one was adopted in which the distributions of $\overline{\theta}$ had standard deviations of about 10°. Distributions with much larger deviations than this resulted in only relatively minor improvements to the fits while distributions with much smaller deviations produced significantly poorer fits.

Figure 6 shows the resulting lightcurve fits and Table III shows the resulting spin state and photometric parameters for the four models considered. The χ^2 values are normalized to the best fit which had an rms error of 0.04 mag. Notice that the spin state parameters are essentially the same as for the homogeneous case. This is an indication that no strong correlation exists between the spin state and photometric inhomogeneities. All four fits are visually reasonable, but the northern lower-bound is statistically a better fit than the other three models. Still, the differences are small enough that it is conceivable that they might be due to discrepancies between the (necessarily) idealized photometric model and real scattering from Castalia's surface rather than to the northern lower-bound model being a more accurate representation of Castalia. This model's very large mean value of $\overline{\theta}$ may hint at such a discrepancy, or it may indicate that the surface of Castalia is, in fact, extremely rough.

Nonetheless, the consistent selection of the northern lower-bound model using three different photometric functions (S-class, homogeneous, inhomogeneous) leads us to conclude that it is likely a better representation of the shape of Castalia than the other models; even so, Castalia is still a clearly bifurcated object (Hudson and Ostro 1995). Moreover, we also interpret this trend as pointing towards a resolution of the mirror ambiguity allowed by the single-date radar data set in favor of the northern model.

It is interesting to note that similar results can be obtained by allowing the single-scattering albedo w to vary spatially instead of $\overline{\theta}$. This is reasonable given the large

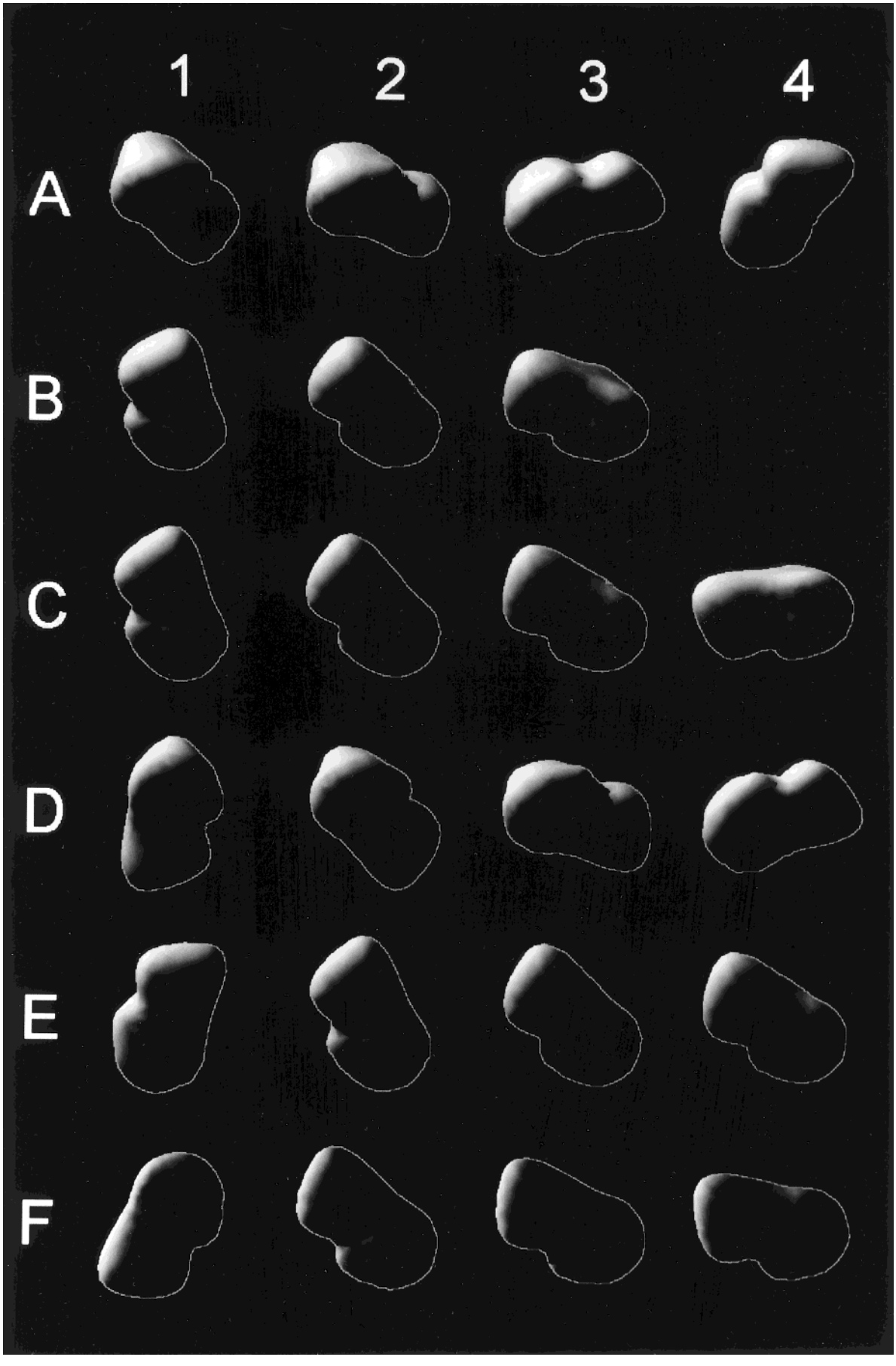
1
2
3
4
A
B
C
D
E
F

phase angles. At a large phase angle the brightness of a surface element can be decreased either by decreasing the intrinsic brightness of the surface material (w) or by increasing the macroscopic roughness ($\overline{\theta}$) and hence shadowing. Definitive resolution of this ambiguity would require data at small phase angles where there is much less sensitivity to roughness. However, as discussed above, spatial variations in $\overline{\theta}$ seem more plausible than variations in w.

Figure 7 illustrates the nature of the $\overline{\theta}$ distributions of the lower bound models. We consider a region to be ''smooth'' if $\overline{\theta}$ there is less than the average value over the surface; otherwise, we consider the region to be ''rough.'' In these renderings smooth regions appear dark while rough regions appear bright. The smoothness features at the object's ends are particularly interesting. They are fairly well correlated between the north and south models and display a tendency to be skewed toward the leading side of the asteroid with respect to its rotation. If direct impacts or spallation effects were to produce clouds of orbiting ejecta, these regions would be most likely to ''sweep up'' those particles, a process which could lead to smooth blanketing. Hence, although no definite statements are possible, it is conceivable that we are seeing evidence in these lightcurves for the effects of a non-uniform distribution of regolith on the surface variation of macroscopic roughness.

It is interesting to note that Castalia's two lobes show no evidence of major qualitative differences in their radar (Hudson and Ostro 1994) or optical properties. If Castalia is a contact binary, as its shape strongly suggests, and that simulations predict should be a frequent outcome of catastrophic collisions (Durda 1996), it may be that the two lobes are samples of the same region of a parent body. It may also be that Castalia is covered with a ''well-gardened'' regolith covering two lobes of similar or dissimilar composition. The possibility of a regolith is suggested by the appearance of relatively large smoothness features in the inhomogeneous models.

Finally, we consider the relationship between Castalia's POS appearance and its lightcurve. In Fig. 8 we plot the observed data (open circles) and selected fit data (filled circles). The POS appearance of Castalia corresponding to the fit data are shown in Fig. 9. Note that only a small fraction of Castalia's surface was illuminated and visible at any time, especially near the end of observations. The lightcurve minima (A1, B2, C2, D2, E3, F3) occurred when one of the lobes eclipsed the other leaving only a minimal cross section illuminated and visible. The maxima (A3, C4, D4, E1) occurred when both lobes were illuminated and visible, i.e., when a ''side'' of the object was facing the Sun. Note how the deeper ''waist'' on one side of the object leads to one maximum being flatter (D4, E1) than the maximum corresponding to the other side (C4, D1) as the more rounded geometry of the lobes in the former case results in less sensitivity to rotation. (Note: Castalia renderings are available on VHS tape (de Jong and Suzuki 1995) and on the world wide web at http://www.eecs.wsu.edu/~hudson/asteroids.html.)

5. CONCLUSION

We have demonstrated that ground-based radar and optical observations can be used together to constrain the shape, spin state, and photometric properties of an asteroid, even with only a few consecutive days of data. Given enough geometric diversity, lightcurves have the potential to resolve the mirror ambiguity which is inherent in a single-date radar data set and thereby solve for the sense of rotation. When combined in this manner, the scientific value of the individual data sets is significantly enhanced. Given the large increase in sensitivity expected with the upgraded Arecibo radar (http://www.naic.edu/) this synergy should play a major role in future studies of near-Earth objects.

ACKNOWLEDGMENTS

Work at WSU was supported by NASA Grant NAGW-4636. Part of this research was conducted at the Jet Propulsion Laboratory, California Institute of Technology, under contract with NASA.

REFERENCES

Belton, M. J. S., J. Veverka, P. Thomas, P. Helfenstein, D. Simonelli, C. Chapman, M. E. Davies, R. Greeley, R. Greenberg, J. Head, S. Murchie, K. Klaasen, T. V. Johnson, A. McEwen, D. Morrison, G. Neukum, F. Fanale, C. Anger, M. Carr, and C. Pilcher 1992. Galileo encounter with 951 Gaspra: First pictures of an asteroid. *Science* **257,** 1647–1652.

de Jong, E., and S. Suzuki 1995. Lightcurves and orbits for asteroid 4769 Castalia, AVC-95-037. Catalog on-line at: http://www.jpl.nasa.gov/archive/vidcat.html.

Durda, D. D. 1996. The formation of asteroidal satellites in catastrophic collisions. *Icarus* **120,** 212–219.

Hapke, B. 1981. Bidirectional reflectance spectroscopy 1. Theory. *J. Geophys. Res.* **86,** 3039–3054.

Hapke, B. 1984. Bidirectional reflectance spectroscopy 3. Correction for macroscopic roughness. *Icarus* **59,** 41–59.

FIG. 9. Plane-of-sky appearances of Castalia model corresponding to fit data points in Fig. 8. The object's silhouette is outlined in each rendering to enable visualization of shadowed regions.

Hapke, B. 1986. Bidirectional reflectance spectroscopy 4. The extinction coefficient and the opposition effect. *Icarus* **67,** 264–280.

Harris, A. W., and D. F. Lupishko 1989. Photometric lightcurve observations and reduction techniques. In *Asteroids II* (R. P. Binzel, T. Gehrels, and M. S. Matthews, Eds.), pp. 39–59. Univer. of Arizona Press, Tuscon.

Harris, A. W., and J. W. Young 1983. Asteroid rotation IV. *Icarus* **54,** 59–109.

Helfenstein, P., J. Veverka, P. C. Thomas, D. P. Simonelli, P. Lee, K. Klaasen, T. V. Johnson, H. Breneman, J. W. Head, S. Murchie, F. Fanale, M. Robinson, B. Clark, J. Granahan, H. Garbeil, A. S. Mcewen, R. L. Kirk, M. Davies, G. Neukum, S. Mottola, R. Wagner, M. Belton, C. Chapman, and C. Pilcher 1994. Galileo photometry of asteroid 951 Gaspra. *Icarus* **107,** 37–60.

Helfenstein, P., J. Veverka, P. C. Thomas, D. P. Simonelli, K. Klaasen, T. V. Johnson, F. Fanale, J. Granahan, A. S. Mcewen, M. Belton, and C. Chapman 1996. Galileo photometry of asteroid 243 Ida. *Icarus* **120,** 48–65.

Hudson, R. S., and S. J. Ostro 1994. Shape of asteroid 4769 Castalia (1989 PB) from inversion of radar images. *Science* **263,** 940–943.

Hudson, R. S., and S. J. Ostro 1995. Shape and non-principal axis spin state of asteroid 4179 Toutatis. *Science* **270,** 84–86.

Lagerkvist, E. I., M. A. Barucci, M. T. Capria, M. Fulchigoni, M. Guerriero, E. Perozzi, and V. Zappala 1987. *Asteroid Photometric Catalog*. The most recent update (1993) is published by the Astronomiska Observatoriet, Uppsala Universitet, Uppsala Sweden. For information on electronic data retrieval contact Per.Magnusson@astro.uu.se (Internet).

Landau, L. D. and E. M. Lifshitz 1976. *Mechanics,* 3rd ed. Pergamon, Oxford.

Magnusson P., M. A. Barucci, J. D. Drummond, K. Lumme, S. J. Ostro, J. Surdej, R. C. Taylor, and V. Zappala 1989. Determination of pole orientations and shapes of asteroids. In *Asteroids II* (R. P. Binzel, T. Gehrels, and M. S. Matthews, Eds.), Univ. of Arizona Press, Tuscon.

Ostro, S. J., J. F. Chandler, A. A. Hine, K. D. Rosema, I. I. Shapiro, and D. K. Yeomans 1989. Radar images of asteroid 1989PB. *Science* **248,** 1523–1528.

Ostro, S. J. 1993. Planetary radar astronomy. *Rev. Modern Phys.* **65,** 1235–1279.

Russell, H. N. 1906. On the light-variations of asteroids and satellites. *Astrophys. J.* **24,** 1–18.

Simonelli, D. P., J. Veverka, P. C. Thomas, and P. Helfenstein 1995. Analysis of Gaspra lightcurves using Galileo shape and photometric models. *Icarus* **114,** 387–402.

Simonelli, D. P., J. Veverka, P. C. Thomas, P. Helfenstein, B. T. Carcich, and M. J. S. Belton 1996. Ida lightcurves: Consistency with Galileo shape and photometric models. *Icarus* **120,** 38–47.

Thomas, P. C., J. Veverka, D. Simonelli, P. Helfenstein, B. Carcich, M. J. S. Belton, M. E. Davies, and C. Chapman 1994. The shape of Gaspra. *Icarus* **107,** 23–36.

Thomas, P. C., M. J. S. Belton, B. Carcich, C. R. Chapman, M. E. Davies, R. Sullivan, and J. Veverka 1996. The shape of Ida. *Icarus* **120,** 20–32.